International Journal of Hydrogen Energy 60 (2024) 601–610

Contents lists available at ScienceDirect

International Journal of Hydrogen Energy

journal homepage: www.elsevier.com/locate/he

Fabrication of $Ni_2O_2(OH)$/CNTs-based electrocatalyst for efficient bifunctional electrocatalytic water splitting

Muhammad Afaq [a], Amal BaQais [b], Eric W. Cochran [c], Sonia Zulfiqar [c,d], Mohammed A. Amin [e], Muhammad Shahid [f], Iqbal Ahmad [g], Sheraz Yousaf [a,*], Muhammad Farooq Warsi [a,**]

[a] Institute of Chemistry, Baghdad-ul-Jadeed Campus, The Islamia University of Bahawalpur, Bahawalpur, 63100, Pakistan
[b] Department of Chemistry, College of Science, Princess Nourah bint Abdulrahman University, P.O. Box 84428, Riyadh, 11671, Saudi Arabia
[c] Department of Chemical and Biological Engineering, Iowa State University, Sweeney Hall, 618 Bissell Road, Ames, Iowa, 50011, United States
[d] Department of Chemistry, Faculty of Science, University of Ostrava, 30. Dubna 22, Ostrava, 701 03, Czech Republic
[e] Department of Chemistry, College of Science, Taif University, P.O. Box 11099, Taif, 21944, Saudi Arabia
[f] Department of Chemistry, College of Science, University of Hafr Al Batin, P.O. Box 1803, Hafr Al Batin, Saudi Arabia
[g] Department of Chemistry, Allama Iqbal Open University, Islamabad, 44000, Pakistan

ARTICLE INFO

Handling Editor: Dr F Gallucci

Keywords:
Electrocatalysis
Water splitting
Electrocatalysts
Bifunctional catalyst
OER
HER

ABSTRACT

Exploring the cost-effective and earth-abundant electrocatalyst for efficient bifunctional activity is very challenging these days. The main reason is very slow OER (oxygen evolution reaction) kinetics as compared with HER (hydrogen evolution reaction). An electrocatalyst with enhanced kinetics towards OER and HER is highly required, which may be attributed to a larger surface area, an increased number of active sites, and lower charge transfer resistance. In this paper, we have reported a very efficient bifunctional $Ni_2O_2(OH)$/CNTs electrocatalyst by a facile ultrasonication route followed by annealing for OER/HER performance in an alkaline solution. The $Ni_2O_2(OH)$/CNTs electrocatalyst exhibits a lower overpotential of 228 mV and 270 mV during OER to accomplish a current density of 40 and 100 $mAcm^{-2}$ while it requires a 368 mV and 418 mV overpotential during HER to achieve a current density of 40 and 100 $mAcm^{-2}$. The prepared $Ni_2O_2(OH)$/CNTs electrocatalyst has a lesser Tafel slope (132 $mVdec^{-1}$; OER, 115 $mVdec^{-1}$; HER) as compared to $Ni_2O_2(OH)$ (239 $mVdec^{-1}$; OER, 124 $mVdec^{-1}$, HER). $Ni_2O_2(OH)$/CNTs exhibit reduced charge resistance, enhanced electrochemical active surface area, greater carrier concentration, and a higher exchange current density, which confirms its superior bifunctional electrocatalytic activity. This work provides an economical and affordable means to prepare superior, efficient bifunctional electrocatalysts for widespread commercial applications.

1. Introduction

There are many common issues all around the world. Among these issues, the few issues are very important. These are energy production and storage and environmental pollution. Researchers are continuously working their efforts to address these issues. The use of fossil fuels for energy production and preservation is one solution to energy shortages that has gained widespread recognition [1–3]. On the other hand, when fossil fuels are burned, they give off harmful gases that contribute directly to pollution and, in the long run, global warming [4,5]. Because of this, it is crucial to phase out fossil fuels in favor of renewable energy sources that are better for the environment [6,7]. Hydrogen is a great choice for making energy in the future because it is light and has a high energy density [8,9]. Hydrogen can be made in several different ways, such as by electrolyzing or photolyzing water, reforming biomass, or burning fossil fuels [10]. Most hydrogen is made through a process called electrolysis [11]. In electrochemical water-splitting reactions, at cathode, the HER takes while the OER takes place at anode. [12–14]. Rare and expensive metals are needed for HER and OER technologies, specifically platinum (Pt) for the electrochemical HER process and iridium and ruthenium dioxide (IrO_2; RuO_2) for the OER process [15–17]. Electrolysis needs more energy because the reactions at the electrode junctions take place slowly. This is because the overpotential is high. To get around the problems with traditional noble metal

* Corresponding author.
** Corresponding author.
E-mail addresses: sherazyousaf2@gmail.com (S. Yousaf), farooq.warsi@iub.edu.pk (M.F. Warsi).

https://doi.org/10.1016/j.ijhydene.2024.02.109
Received 4 December 2023; Received in revised form 26 January 2024; Accepted 8 February 2024

electrodes, we need to find a catalyst that is effective, earth-abundant, cheap, and long-lasting [18,19]. Numerous studies have demonstrated the potential of metal nitrides, metal oxides, metal hydroxides, metal oxide hydroxides, metal layer double hydroxides, metal sulfides, and transition metal dichalcogenides as electrocatalysts, but none of them have been able to match the stability and long-term catalytic efficiency of catalysts made from noble metals [20–23]. In the same electrochemical device, the base electrode must therefore effectively serve as a dual-functional catalyst material for both HER and OER processes [24]. Each electrocatalyst requires a different preparation process, which raises the price of both the engineering and manufacturing phases. An electrode material with a large surface area and built-in catalytic activity would be ideal for splitting water [25]. It is well known that transition metals like Au, Ni, Co, Fe, and Cu have the best electrocatalytic properties after the platinum group metals [26]. Ni-based alloys and nanocomposite materials have drawn more consideration because of their potential in both alkaline and acidic solutions. The overpotential of Ni-based composites is low, and they are also resistant to corrosion [27,28].

The nickel oxide hydroxide ($Ni_2O_2(OH)$) as an electrocatalyst for water splitting has also received significant attention due to its material potential. There is a lot of surface area available for electrocatalytic reactions on $Ni_2O_2(OH)$ because of its layered structure. Their electrocatalytic activity and efficiency for water-splitting reactions, especially the OER, are improved as a result of layered structure. The OER reaction is an essential part of the water-splitting reaction, but it is a difficult reaction that calls for a lot of overpotential to be active. $Ni_2O_2(OH)$ are easy to synthesize, abundant, and inexpensive, making them preferable over electrocatalysts based on precious metals like platinum for use in large-scale applications. $Ni_2O_2(OH)$ activity for the HER is comparable to that of $Ni(OH)_2$ and NiO(OH), but lower than that of some other electrocatalysts [29,30]. Researchers have attempted a variety of methods, including doping with other metals and integrating them into composite materials with other materials like carbon nanotubes (CNTs), to increase their activity for HER [31].

CNTs are appealing candidates for use as a support material for electrocatalysts due to their high electrical conductivity, massive surface area, and unique structural properties [2,32]. Composites for electrochemical water splitting that contain CNTs offer multiple distinct advantages. To begin with, CNTs have high electrical conductivity, which helps with charge transfer in the water-splitting process. This increases the entire process's efficiency by contributing to electron transfer. Secondly, the incorporation of CNTs into composites improves the stability and longevity of the electrode material. Also, it ensures that it will work well for a long time. The unique structure of CNTs provides a large surface area, which makes active water-splitting sites more available and thus increases efficiency. In the last analysis, CNTs are good catalyst supports. By helping water-splitting reactions involve active species, this also promotes the catalytic activity of the composite electrode material as a whole. When CNTs are incorporated with $Ni_2O_2(OH)$, their electrocatalytic properties for both OER and HER are enhanced. The resulting composite material can show synergistic effects, in which the combined properties of the two materials improve the electrocatalytic activity as a whole. The $Ni_2O_2(OH)$ nanoparticles can be stabilized by the CNTs, increasing their longevity and stability during electrocatalytic reactions, and the CNTs might offer a conductive pathway for electron transfer [33].

$Ni_2O_2(OH)$ can be made using a variety of techniques. In one of the usual methods used, when nickel hydroxide is precipitated from aqueous nickel salt solutions in another preparation, thermal treatment leads to the precipitation of $Ni_2O_2(OH)$. Another method is hydrothermal synthesis which involves placing nickel precursors in an aqueous solution and sealing them at elevated temperatures and pressures to promote the synthesis of $Ni_2O_2(OH)$. Moreover, deposition by electrochemical techniques includes first electrodeposited and then oxidized nickel on a conductive substrate so it turns into $Ni_2O_2(OH)$. Finally, the preparation of $Ni_2O_2(OH)$ can also be controlled by using sol-gel method which requires a sol containing nickel ions and gelling it, thereafter thermally treating this varied range of synthesis procedures makes it feasible to tune the properties of nickel hydroxide for usage as a catalyst in industry, energy storage, and electrochemical sensors. There are benefits and drawbacks associated with each of them. Ultrasonication stands out from these methods because the chemical effects result from acoustic waves. The interfacial implosion of bubbles in the solution causes a sudden pressure signal and a high temperature in the solution. This acoustic cavitation resulted in localized, extreme micro-mixing [34]. The rate of the ultrasonic chemical reaction is so high because of the numerous times the reactant molecules collide, which is one of the benefits of sonochemical synthesis. This method does not require the use of any additional external reagents, such as capping or surfactant reagents. Additionally, it is because the products of sonochemical synthesis are highly pure and the reaction environment is more environmentally friendly. Furthermore, it is simple to control the size distribution of products by simply changing the ultrasound frequency and power [35–38].

In this study, $Ni_2O_2(OH)$ and $Ni_2O_2(OH)$/CNTs electrocatalysts were fabricated by ultrasonication, followed by annealing of the materials. The resultant $Ni_2O_2(OH)$/CNTs exhibits excellent catalytic performance for electrochemical water-splitting reactions (HER/OER) in an alkaline medium. The notable electrocatalytic performance of $Ni_2O_2(OH)$/CNTs catalyst can be primarily attributed to its distinctive porous structure, excellent conductivity, and expansive surface area, which are derived from the presence of carbon nanotubes.

2. Experimental Section

2.1. $Ni_2O_2(OH)$ and $Ni_2O_2(OH)$/CNTs Synthesis

A quick, low-cost, and easy technique of ultrasonic irradiation was used to prepare the $Ni_2O_2(OH)$ and $Ni_2O_2(OH)$/CNTs electrocatalysts. 6.87 mmol $Ni(NO_3)_2{\cdot}6H_2O$ and 24 g/20 mL polyethylene glycol (PEG) were co-dissolved in a crucible. Two hours of ultrasonic treatment was applied to the mixed solution. Afterward, the ultrasonically treated mixed solution was annealed at 700 °C for 2 h. The resultant $Ni_2O_2(OH)$ material was acquired after annealing. The $Ni_2O_2(OH)$/CNTs nanohybrid was then synthesized by using a standard ultrasonication method. The as-prepared $Ni_2O_2(OH)$ and CNTs suspension (1mg/1 mL) were co-dissolved (9:1) and placed in an ultrasonic cleaner bath for 120 min of ultrasonic processing, thereafter obtained mixture was dried at 80 °C and then used for further electrocatalytic applications. The overall synthesis mechanism and its electrochemical characterization are pictorially represented in Fig. 1.

2.2. Materials characterization

$Ni_2O_2(OH)$ and $Ni_2O_2(OH)$/CNTs samples were characterized by Lab XRD-6100 powder X-ray diffraction (XRD) to determine their crystal phase, structure, and crystallite size. In the 20–60° wavelength range, kα radiations from a Cu source with a wavelength of 1.54 Å were utilized in the analysis. The molecular composition and chemical bonding of the electrocatalysts were monitored using Fourier transform infrared spectroscopy (FTIR; IR affinity 1S). The fabricated samples were analyzed by employing a scanning electron microscope (SEM; Inspect S50 FEI) to determine their structure and surface morphology. The XPS measurements were performed using a Kratos Amicus/ESCA 3400 instrument. The samples were irradiated with 240 W unmonochromated Mg Kα X-rays, and photoelectrons emitted at 0° from the surface normal were energy analyzed using a DuPont type analyzer. The pass energy was set at 150 eV. CasaXPS was used to process raw data files.

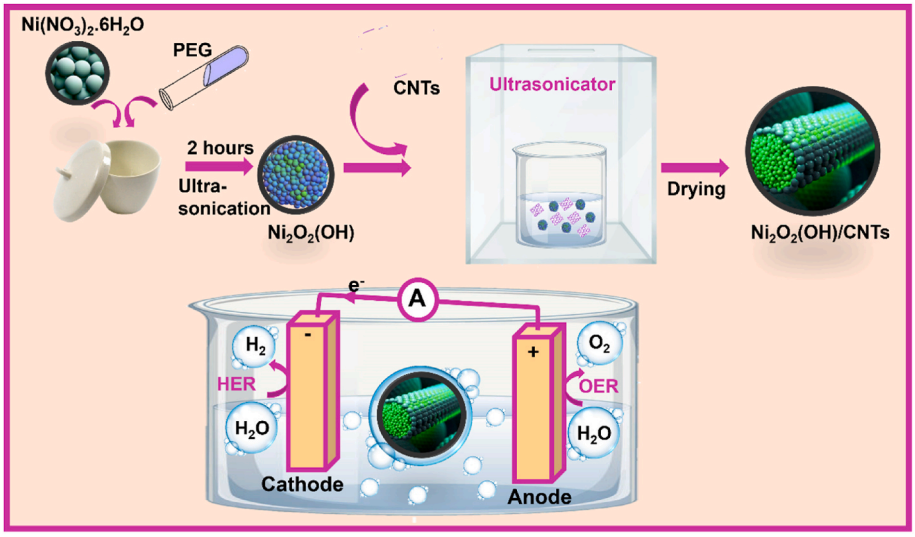

Fig. 1. Synthesis and mechanism scheme of low-cost bifunctional $Ni_2O_2(OH)$/CNTs electrocatalyst for OER/HER electrocatalysis.

2.3. Preparation of electrodes

The 1 cm × 1 cm measured substrate material (carbon fiber cloth, CFC) was washed firstly with ethanol, acetone, and deionized water. The catalyst ink was prepared by sonicating the 15 mg of catalyst into 100 μL of deionized water for 2 h. The prepared catalyst ink was then mounted on a premeasured CFC selective area by drop casting method.

2.4. Electrochemical assessments

The electrocatalytic activities of $Ni_2O_2(OH)$ and $Ni_2O_2(OH)$/CNTs catalysts were studied by using a Gamry Interface 5000E electrochemical workstation. For electrochemical analysis, three-electrode configurations were established: a reference (mercury/mercury oxide; Hg/HgO), a counter (platinum foil; Pt), and a working (modified and unmodified CFC) electrode. The electrolyte solution of 1 M KOH was used in the electrochemical tests. The OER activity of $Ni_2O_2(OH)$, $Ni_2O_2(OH)$/CNTs, and RuO_2 electrocatalysts were evaluated by using linear sweep voltammetry (LSV) polarization curves at a sweeping rate of 5 mVs^{-1}. To better understand the HER process, LSV recording of as-synthesized materials were made at 5 mVs^{-1} and compared to LSV recordings of CFC, CFC with binder, and Pt foil. In light of the LSV curve, we can determine the Tafel plot (log j vs overpotential) by using the equation; $\eta = b \log j + a$, where η represents overpotential, j denotes current density, b refers to tafel slope and a is the intercept [39]. The obtained $E_{Hg/HgO}$ was converted into reversible hydrogen electrode potential by using this equation: $E_{RHE} = E_{Hg/HgO} + 0.098 + 0.059$ pH and the corresponding overpotential (OP) in terms of OER was estimated by subtracting the thermodynamic potential value, which is 1.23 V from the reference electrode potential ($E_{Hg/HgO}$) [40]. The electrochemical active surface area (ECSA) of resultant samples was quantified using cyclic voltammograms (CV) at various scan rates, with the most common being the non-Faradic current region at CV fixed potential range. The ECSA of both $Ni_2O_2(OH)$ and $Ni_2O_2(OH)$/CNTs materials are calculated by dividing the C_{dl} value of each sample by a specific capacitance value (0.040 $mFcm^{-2}$) [41]. Nyquist plots from electrochemical impedance spectroscopy (EIS) tests were considered to further evaluate the catalytic efficiency of as-fabricated materials. Chrono-potentiometric analysis was performed to assess the stability of the electrocatalyst for OER electrocatalysis, while chronoamperometric analysis was considered to check the stability of the material during HER.

3. Results and discussion

3.1. XRD studies

The XRD technique was performed to analyze the composition, crystal system, and crystal structure of the prepared samples. The diffraction patterns of prepared $Ni_2O_2(OH)$ and $Ni_2O_2(OH)$/CNTs nanostructures are displayed in Fig. 2. The diffraction peaks at 2θ = 30.2°, 31.46°, 35.18°, 40.38°, 44.26°, 45.27°, 50°, 53.6°, 56.28°, and 58.46° are well-indexed with crystal planes (104), (011), (200), (203), (114), (015), (212), (116), (302), and (215) respectively. The diffraction patterns for $Ni_2O_2(OH)$ correspond to an orthorhombic crystal system with space group Pmnn (JCPDS# 01-084-1459). The peak at 29° in the XRD of $Ni_2O_2(OH)$/CNTs nanocomposites corresponds to the (102) diffraction plane of water molecules, as indicated by standard JCPDS#00-016-0598. A clear diffraction spike at 25.7° is observed, which is the characteristic peak of CNTs [42] in the XRD patterns of $Ni_2O_2(OH)$/CNTs which confirms the successful formation of a binary nanocomposite.

The X-ray density of as-prepared $Ni_2O_2(OH)$ was calculated by employing the following equation [43].

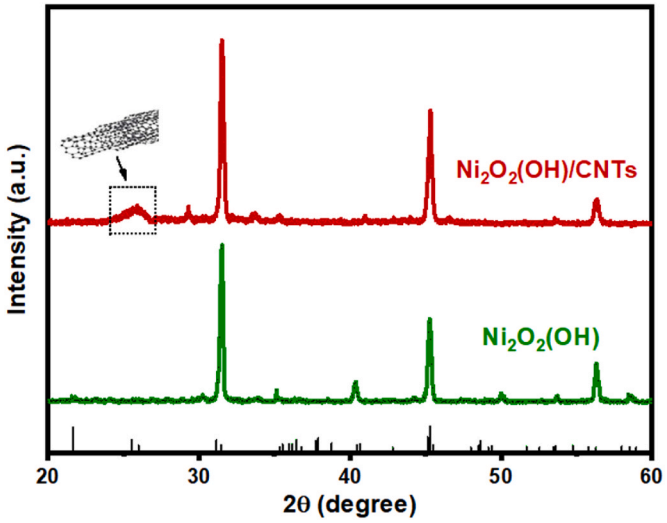

Fig. 2. XRD patterns of $Ni_2O_2(OH)$ and $Ni_2O_2(OH)$/CNTs.

$$d_x = \frac{Z \times M}{N_A \times V} \quad (1)$$

Whereas d_x denotes the X-ray density of a given material, M is the molar mass of the material, Z represents the total number of molecules present in a unit cell volume, V shows the total volume of a unit cell, and N_A denotes Avogadro's number. The calculated d_x of $Ni_2O_2(OH)$ is 5.409 gcm^{-3}.

The specific surface area (SSA) of $Ni_2O_2(OH)$ was determined by using the following equation [44]:

$$SSA = A_p / d_x \times V_p \quad (2)$$

In this equation, the specific area of the particle is denoted by A_p, the volume of the particle is represented by V_p and d_x refers to the X-ray density of material. The fabricated $Ni_2O_2(OH)$ has a greater specific surface area (399.68 m^2g^{-1}), which is calculated by using the above equation. The higher SSA of $Ni_2O_2(OH)$ is due to its sonochemical synthesis, as the acoustic cavitation generated during sonochemical synthesis promotes the formation of small and uniform nanoparticles with a high surface area-to-volume ratio.

The crystallite size of the prepared $Ni_2O_2(OH)$ was also determined by using the Debye-Scherrer formula [45]. The resultant $Ni_2O_2(OH)$ estimated crystallite size is given in Table 1.

The dislocation density of the resultant $Ni_2O_2(OH)$ was computed by using the following relation.

$$\delta = 1/D^2 \quad (3)$$

Where δ refers to dislocation density and D stands for crystallite size. The dislocation density of the $Ni_2O_2(OH)$ sample is 0.000826 nm^{-2}.

3.2. FTIR analysis

FTIR study was done to examine the molecular nature and composition of the as-prepared $Ni_2O_2(OH)$ material. All FTIR spectra were recorded at room temperature. The FTIR study was carried out in wavenumber range from about 500 to 4000 cm^{-1}. FTIR spectra of prepared compound $Ni_2O_2(OH)$ and its composite with carbon nanotubes (CNTs) are shown in Fig. 3. The absorption band located at 651 cm^{-1} corresponds to the metal-oxygen vibrational mode [46]. The appearance of bands between 800 and 1800 cm^{-1} range could be assigned to anionic impurities that may not have been completely removed during the washing. The bands located at 1095 cm^{-1}, 1199 cm^{-1}, and 1459 are attributed to carbonate group stretching vibrations, which may appear from the adsorption of atmospheric CO_2 onto the material [46,47]. Detected band around 1694 cm^{-1} was ascribed to the bending vibrations of water molecules [48]. Two bands observed in the FTIR spectrum at 3460 cm^{-1} and 3734 cm^{-1} could be allocated to different stretching modes of OH [46]. FTIR spectra of $Ni_2O_2(OH)$/CNTs reveals that composite material has nearly the same features as the bare $Ni_2O_2(OH)$ material with variations in band intensity and positions. These changes indicate the formation of the composite material, signifying interactions between the $Ni_2O_2(OH)$ and CNTs components.

Table 1
XRD parameters of as-fabricated $Ni_2O_2(OH)$.

Sr. No.	Parameters	$Ni_2O_2(OH)$
1.	Crystal phase	Orthorhombic
2.	Crystallite size (nm)	34.8
3.	Dislocation density (nm^{-2})	0.000826
4.	Lattice constant a(Å)	5.07
5.	Lattice constant b(Å)	2.9
6.	Lattice constant c(Å)	13.9
7.	Cell volume $(Å)^3$	204.37
8.	Specific surface area (m^2g^{-1})	399.68
9.	X-ray density (gcm^{-3})	5.409

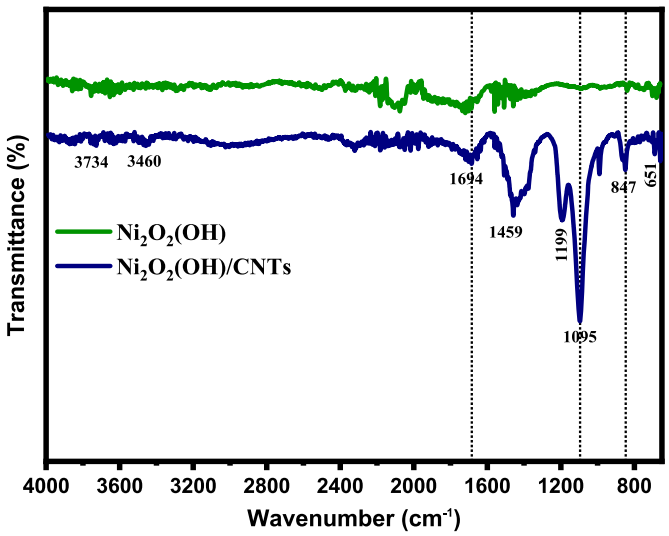

Fig. 3. FTIR spectra of $Ni_2O_2(OH)$ and $Ni_2O_2(OH)$/CNTs.

3.3. SEM analysis

The SEM images are recorded through the morphological analysis of as-prepared samples. Fig. 3(a) and (b) represent SEM images of $Ni_2O_2(OH)$ and $Ni_2O_2(OH)$/CNTs, respectively. The SEM images reveal various particles of $Ni_2O_2(OH)$ in Fig. 4(a). Some particles appear as elongated nanoplates, exhibiting a thin, plate-like morphology. These nanoplates are elongated along a particular crystallographic direction, resulting in an anisotropic shape. Intermingled with the nanoplates are polyhedral-shaped particles. These particles have well-defined, geometric shapes with multiple facets, resembling polyhedrons. The nanoplates and polyhedral particles are distributed throughout the SEM micrograph, creating a heterogeneous population of $Ni_2O_2(OH)$ particles. Fig. 4(b) shows the clear presence of thread-like structures in $Ni_2O_2(OH)$, which confirms the formation of CNTs-based composites. In the $Ni_2O_2(OH)$/CNTs sample, the lateral sides of plate-like structures are also visible, while polyhedron-like structures are covered by a dense network of CNTs, indicating a tailored architecture promoting enhanced surface area and active sites for electrocatalytic activity.

3.4. X-ray photoelectron spectroscopic (XPS) analysis

Exploring the surface chemical composition of the as-synthesized $Ni_2O_2(OH)$/CNTs involved a thorough investigation through X-ray photoelectron spectroscopy (XPS). The high-resolution curve-fitted XPS peaks corresponding to C 1s, O 1s, and Ni 2p are delineated in Fig. 5 (a–c). In Fig. 5(a), the C 1s core level presents a nuanced breakdown with four components identified as C═C at 284.4 eV, C–H at 285.3 eV, C═O at 286.7 eV, and O–C═O at 289.0 eV [49]. Analysis of the O 1s XPS spectra in Fig. 5(b) reveals three distinct bound states (M − O, oxygen defects, and O–H) associated with lattice oxygen, deficient oxygen sites, and C–O bonds within the carbon matrix or arising from the inevitable physical adsorption of water molecules on the surface [50, 51].

The high-resolution XPS spectrum of Ni 2p (Fig. 5(c)) presents a detailed insight into the electronic structure of nickel in the synthesized $Ni_2O_2(OH)$/CNTs. Two spin-orbit doublets at binding energy values of 855.8 and 873.4 eV are discerned, featuring a spin energy separation of 17.6 eV, indicative of Ni 2p3/2 and Ni 2p1/2 components. The peaks at 861.7 and 879.6 eV are identified as the shake-ups of Ni 2p3/2 and Ni 2p1/2, respectively, providing valuable information on the chemical environment and electronic configuration of nickel within the material [52]. This comprehensive XPS analysis not only defines the elemental composition but also explores the chemical states and bonding

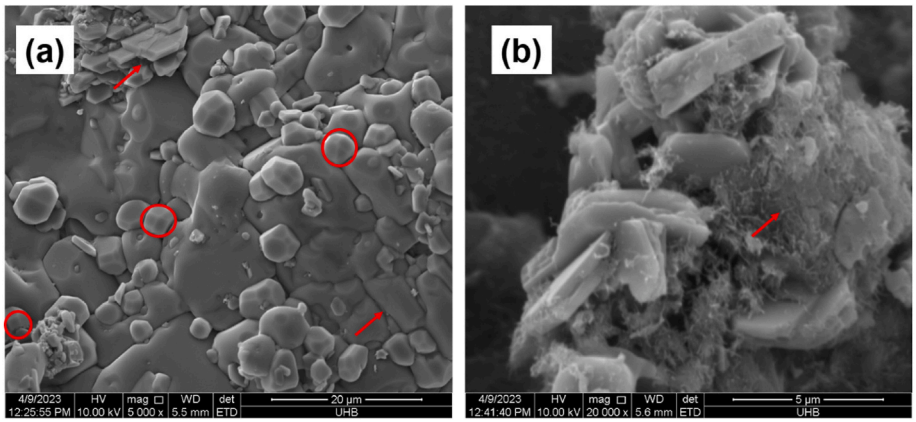

Fig. 4. SEM images of (a) $Ni_2O_2(OH)$ and, (b) $Ni_2O_2(OH)$/CNTs.

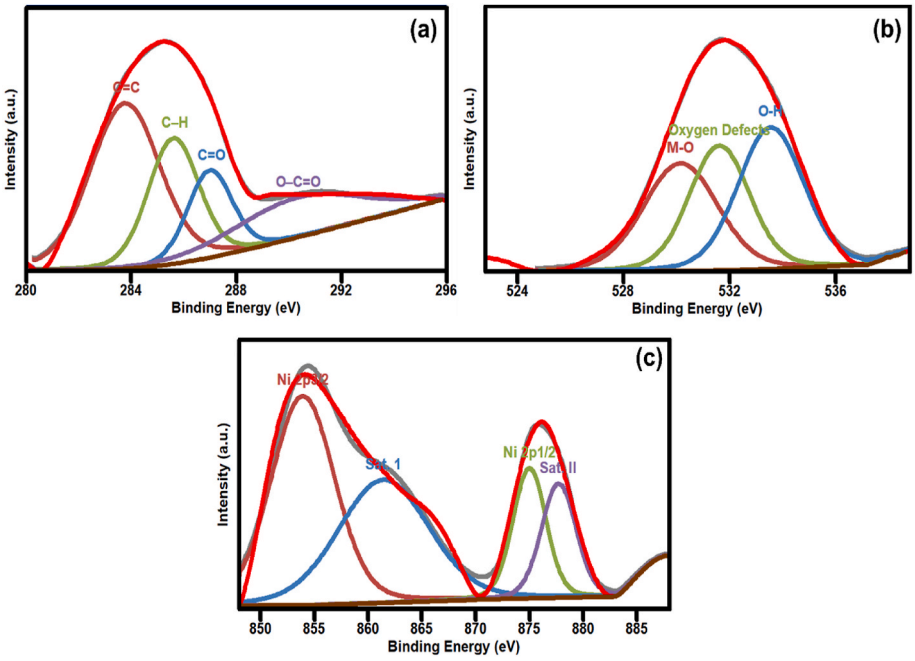

Fig. 5. XPS spectra of $Ni_2O_2(OH)$/CNTs (a) C 1s, (b) O 1s and (c) Ni 2p.

configurations, thereby advancing our understanding of the material's intricate properties.

3.5. OER and HER studies

Cyclic voltammetry profiles were used to figure out the double-layer capacitance (C_{dl}) so that the active sites of electrocatalysts could be evaluated. Fig. 6 represents C_{dl} plots (I *vs.* scan rate) of as-fabricated materials. The average C_{dl} of $Ni_2O_2(OH)$ and $Ni_2O_2(OH)$/CNTs samples was calculated as 0.165 and 0.24 cm^{-2}, respectively. The $Ni_2O_2(OH)$/CNTs catalyst has a higher value of average C_{dl} than the corresponding $Ni_2O_2(OH)$ which demonstrates greater exposure of active sites for OER/HER. The ECSA of as-prepared samples was also determined by using the average C_{dl} values and is presented in Table 3. The ECSA was assumed to be proportionally correlated with the catalytic efficiency. The greater ECSA value of the $Ni_2O_2(OH)$/CNTs catalyst indicates that it provides enormous surface area and active sites for intrinsic electrocatalytic activities as compared to its counterpart.

LSV was employed with a standard three-electrode configuration in an alkaline medium at a potential window of 1.0–1.8 V (*vs.* RHE) to measure the electrochemical OER activities of the as-prepared materials (Fig. 7(a)) and determine the synergistic effects of $Ni_2O_2(OH)$ and $Ni_2O_2(OH)$/CNTs composites. The onset potential of $Ni_2O_2(OH)$/CNTs (1.46 V *vs.* RHE) is lower than the pristine $Ni_2O_2(OH)$ (1.49 V *vs.* RHE). The $Ni_2O_2(OH)$/CNTs requires 228 mV of overpotential to deliver the current density of 40 $mAcm^{-2}$ which is much lesser than $Ni_2O_2(OH)$ (249 mV at the current density of 40 $mAcm^{-2}$) and RuO_2 (270 mV at 40 $mAcm^{-2}$). The $Ni_2O_2(OH)$/CNTs requires 270 mV of overpotential to attain the higher current density of 100 $mAcm^{-2}$ which is much lesser than $Ni_2O_2(OH)$ which requires 300 mV and RuO_2 needs 310 mV of overpotential at the current density of 100 $mAcm^{-2}$. While RuO_2 requires more overpotential to reach a higher current density as compared to others. It indicates the higher OER activity of carbon nanotube-based electrocatalysts. To evaluate the kinetics of electrocatalysts, Tafel slopes are calculated from the Tafel plots as presented in Fig. 7(b). The calculated Tafel slopes of $Ni_2O_2(OH)$, $Ni_2O_2(OH)$/CNTs, and RuO_2 are 239, 132, and 129 $mVdec^{-1}$, respectively. The lesser Tafel slope and overpotential value of $Ni_2O_2(OH)$/CNTs than its counterpart demonstrate that it has more efficient charge kinetics, faster electron mobility, and excellent intrinsic OER activity. The long-term stability of the electrocatalyst is also an important parameter to analyze its electrochemical properties. The stability of the OER $Ni_2O_2(OH)$/CNTs

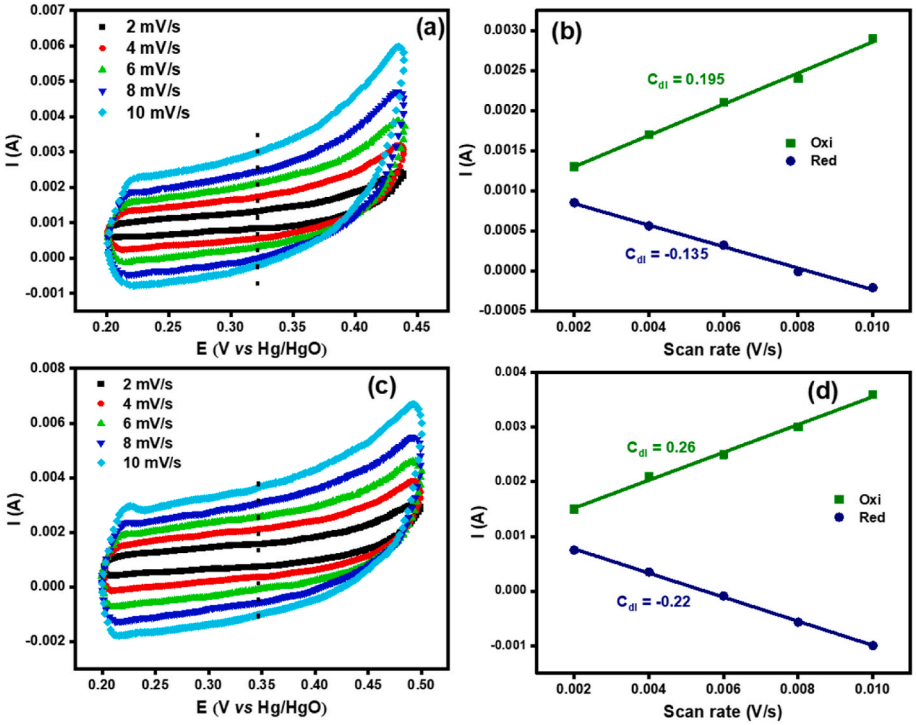

Fig. 6. Cyclic voltammograms of electrocatalysts with varying non-faradaic current regions at various scan rates; (a–b) bare $Ni_2O_2(OH)$ and (c–d) $Ni_2O_2(OH)$/CNTs.

Table 2
Parameters for the evaluation of bifunctional electrocatalytic activity of prepared materials.

Sr. No.	Materials	Tafel slope ($mVdec^{-1}$)		Overpotential (mV)	
		OER	HER	OER	HER
1.	**$Ni_2O_2(OH)$**	239	124	$\eta_{40} = 249$ $\eta_{100} = 300$	$\eta_{40} = 471$ $\eta_{100} = 519$
2.	**$Ni_2O_2(OH)$/CNTs**	132	115	$\eta_{40} = 228$ $\eta_{100} = 270$	$\eta_{40} = 368$ $\eta_{100} = 418$
3.	**RuO_2**	129	–	$\eta_{40} = 270$ $\eta_{100} = 310$	– –
4.	**Pt foil**	–	76	– –	$\eta_{40} = 157$ $\eta_{100} = 227$

Table 3
Experimental parameters for bifunctional activity evaluation of $Ni_2O_2(OH)$ and $Ni_2O_2(OH)$/CNTs electrocatalysts.

Sr. No.	Parameters	$Ni_2O_2(OH)$	$Ni_2O_2(OH)$/CNTs
1.	Average C_{dl} (cm^{-2})	0.165	0.24
2.	ECSA (cm^2)	4.13	6
3.	R_{ct} (Ω)	5.5	2.9
4.	j^o ($mAcm^{-2}$)	1.167	2.214
5.	E_{fb} (V)	0.61	0.55
6.	$N_D \times 10^{22}$ (cm^{-3})	7.66	14.7

electrocatalyst was further assessed by chrono-potentiometric measurements for 5 h at a fixed value of current density of 40 $mAcm^{-2}$ as depicted in Fig. 7(d). It indicates that there is no significant change in the overpotential of the electrocatalyst during the 5 h stability test, which makes it an excellent material for large-scale applications.

To assess the dual-purpose nature of the synthesized catalysts, their performance in a HER setup was measured in an alkaline solution using LSV polarization curves at a potential range of 0 to −0.7 V (*vs.* RHE). Fig. 8(a) represents the HER polarization curves of as-prepared samples, Pt foil and CFC. The current density of −40 $mAcm^{-2}$ and -100 $mAcm^{-2}$ was achieved by $Ni_2O_2(OH)$/CNTs, which requires a very low overpotential of 368 mV and 418 mV than its counterpart $Ni_2O_2(OH)$ (471 mV and 519 mV of overpotential at -40 $mAcm^{-2}$ and -100 $mAcm^{-2}$). While state-of-the-art Pt foil attains a current density of -40 $mAcm^{-2}$ and -100 $mAcm^{-2}$ by requiring an overpotential of 157 mV and 227 mV. The CFC polarization curves demonstrate that they don't get involved during the HER process. The electrocatalytic kinetics can be deduced by analyzing the Tafel slope values (Fig. 8(b)). The calculated Tafel slope (115 $mVdec^{-1}$) of $Ni_2O_2(OH)$/CNTs was lesser as compared to the other sample (124 $mVdec^{-1}$). This indicates that $Ni_2O_2(OH)$/CNTs has a favorable process in the HER reaction pathway and excellent intrinsic activity. The Tafel slope of the $Ni_2O_2(OH)$/CNTs catalyst suggests HER proceeds via the Volmer-Heyrovsky pathway. The durability of $Ni_2O_2(OH)$/CNTs catalyst material was investigated by performing a chronopotentiometry test for 5 h at an overpotential of 368 mV (vs. RHE) for HER electrocatalysis as shown in Fig. 8(d). The chronopotentiometry curve demonstrates a minor change in current density for long time duration which means the electrocatalyst material is efficient and stable for HER electrocatalysis. The results revealed that the design and construction of a CNTs-based-$Ni_2O_2(OH)$ electrocatalyst with enormous active sites, faster kinetics, and excellent charge mobility significantly strengthened its HER activity. Moreover, the bifunctional electrocatalytic activity of prepared materials is summarized in Table 2.

EIS analysis was considered to get insight into kinetics and the charge-transfer resistance (R_{ct}). The Nyquist plots of samples were fitted with a modified Randles circuit, as shown in the inset of Fig. 9. The measured R_{ct} values of $Ni_2O_2(OH)$ and $Ni_2O_2(OH)$/CNTs samples are 5.5 Ω and 2.9 Ω, respectively. The lower R_{ct} value of $Ni_2O_2(OH)$/CNTs is significantly lower than that of bare $Ni_2O_2(OH)$ revealing fast electron transport for the electrocatalytic reaction. The oxygen vacancy formation in $Ni_2O_2(OH)$/CNTs with the tube-like support significantly improves its electrical conductivity, as shown by the R_{ct} comparison with $Ni_2O_2(OH)$. The following equation was used to find the exchange current density (j^o) parameter for the materials: $j^o = RT/nFA\ (\theta')$, where T denotes absolute temperature, n represents the number of electrons, A refers to the geometric area of the electrode surface, F shows Faraday's constant, and R ascribes the charge transfer resistance of the electrode/electrolyte interphase. The calculated exchange current density of

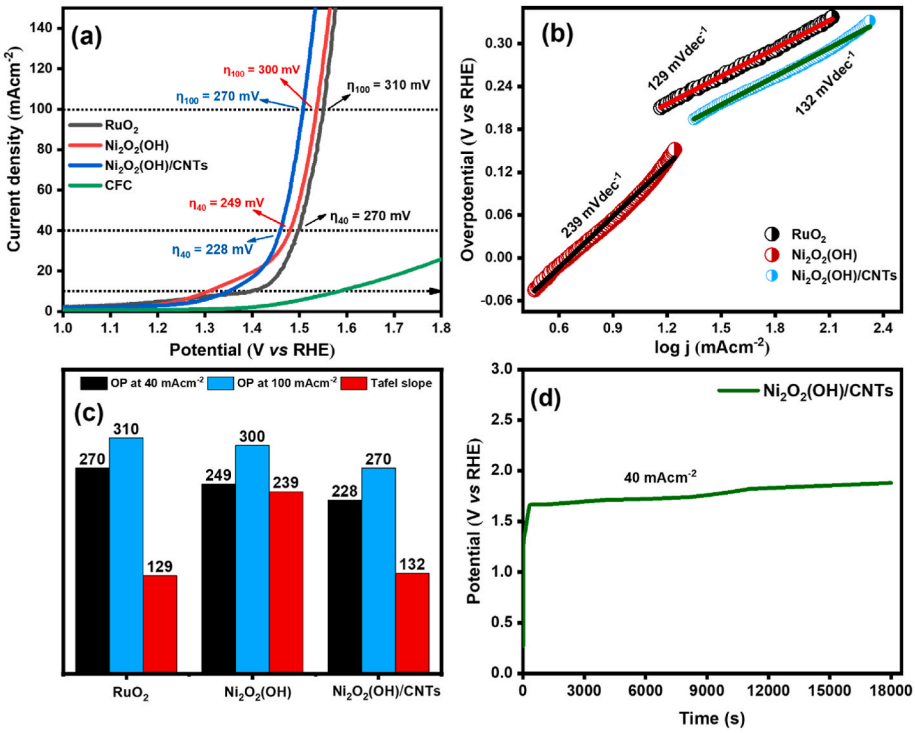

Fig. 7. Representation of OER electrocatalysis results; (a) LSV curves taken at 5 mV/s (b) their corresponding Tafel slope (c) overpotential and Tafel slope bar graphs of RuO_2, $Ni_2O_2(OH)$ and $Ni_2O_2(OH)$/CNTs electrocatalysts and, (d) Chrono-potentiometric curve of $Ni_2O_2(OH)$/CNTs electrocatalyst at 40 $mAcm^{-2}$ during 5 h of OER electrocatalysis.

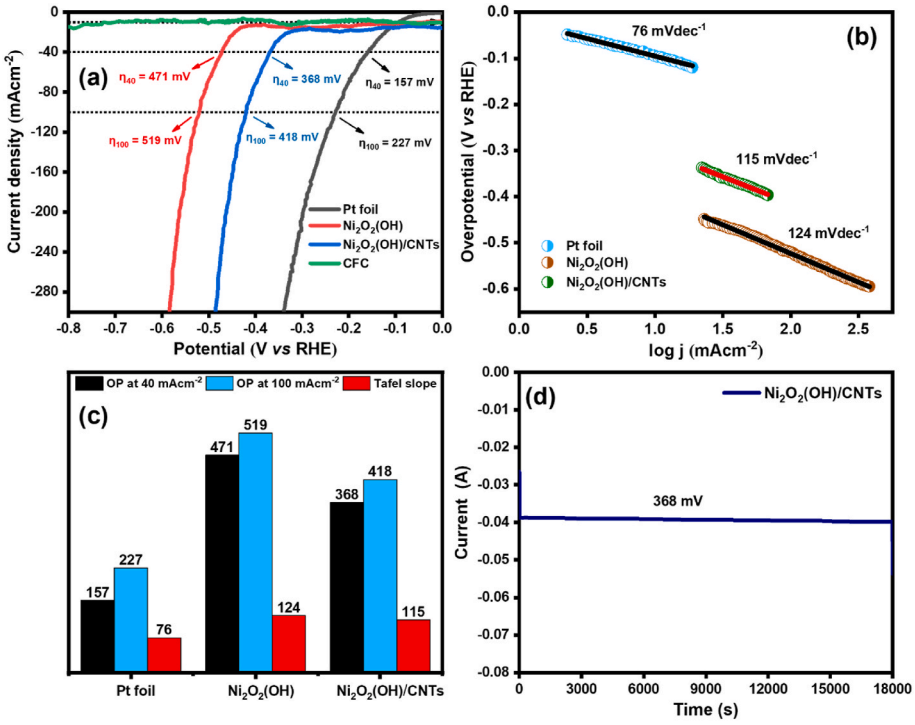

Fig. 8. Illustration of HER electrocatalysis (a) LSV curves taken at 5 mV/s (b) their conforming Tafel slope plot (c) overpotential and Tafel slope comparison bar graph of as-prepared electrocatalysts and, (d) Chronoamperometric curve of a $Ni_2O_2(OH)$/CNTs at 368 mV during 5 h of HER electrocatalysis.

$Ni_2O_2(OH)$ and $Ni_2O_2(OH)$/CNTs is displayed in Table 3. The higher j^o value of $Ni_2O_2(OH)$/CNTs is because of its enhanced intrinsic activity for OER and HER and rapid charge transport kinetics as compared to $Ni_2O_2(OH)$.

Mott-Schottky analysis was conducted to evaluate the flat band potential (E_{fb}) and carrier concentration (N_D) of $Ni_2O_2(OH)$ and $Ni_2O_2(OH)$/CNTs electrocatalysts (Fig. 10). This analysis provides indirect information about the presence of oxygen vacancies. Mott-

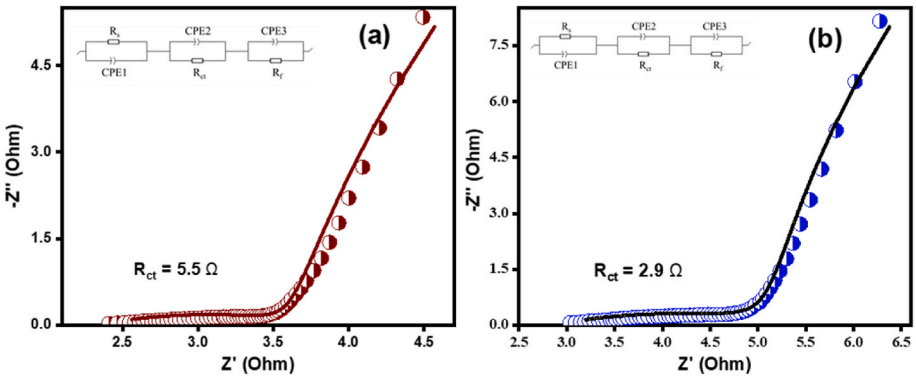

Fig. 9. EIS plots of as-synthesized: (a) bare $Ni_2O_2(OH)$ and (b) $Ni_2O_2(OH)$/CNTs electrocatalysts.

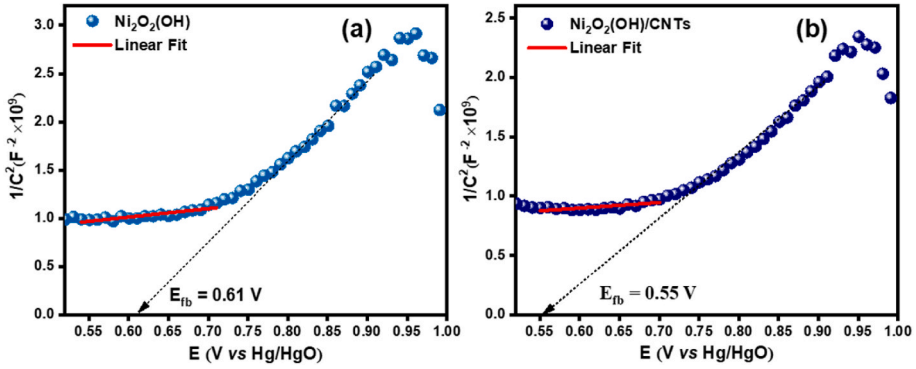

Fig. 10. Mott Schottky analysis of prepared electrocatalysts; (a) $Ni_2O_2(OH)$ and, (b) $Ni_2O_2(OH)$/CNTs.

Schottky tests were considered to observe the electrical properties of the solid-liquid interface. The E_{fb} of $Ni_2O_2(OH)$/CNTs was calculated to be 0.55 V, which is significantly lower as compared to $Ni_2O_2(OH)$. The shift towards a lower potential suggests that the presence of CNTs in the composite affects the electronic properties of $Ni_2O_2(OH)$, potentially altering its catalytic activity for water splitting. Furthermore, another important parameter, N_D of prepared samples has been calculated for the assessment of oxygen vacancies. The $Ni_2O_2(OH)$/CNTs catalyst has a higher calculated carrier concentration compared to $Ni_2O_2(OH)$ as presented in Table 3. This suggests that the presence of CNTs in the composite enhances the formation of oxygen vacancies or promotes electron transfer processes. The increased carrier concentration implies an improved charge transport capability, which can be beneficial for catalytic reactions such as water splitting. Oxygen vacancies in metal oxide materials, such as $Ni_2O_2(OH)$, are lattice defects where oxygen atoms are missing from the crystal structure. These vacancies can act as active sites for electrochemical reactions, including water splitting. The higher carrier concentration in $Ni_2O_2(OH)$/CNTs indicates a higher density of oxygen vacancies, likely due to the presence of CNTs, which promotes defect formation. The reduced flat band potential and higher carrier concentration in $Ni_2O_2(OH)$/CNTs suggest that the presence of CNTs affects the electronic properties and may enhance the catalytic activity for water splitting, potentially impacting electrochemical water splitting reactions (OER/HER). Moreover, the comparison of the current study with the different electrocatalysts synthesized by various strategies from the literature is shown in Table 4.

4. Conclusions

Herein, $Ni_2O_2(OH)$ and $Ni_2O_2(OH)$/CNTs electrocatalysts were synthesized using an easy, simple, and economical ultrasonication method. The prepared material's electrochemical performance was assessed by

Table 4
Comparative studies of the bifunctional $Ni_2O_2(OH)$/CNTs electrocatalyst with previously reported literature.

Electrocatalysts	Electrolyte	Method of synthesis	Overpotential (mV)		Tafel slope ($mVdec^{-1}$)		Ref.
			OER	HER	OER	HER	
$Ni_2O_2(OH)$/CNTs	1 M KOH	Ultrasonication route	η_{40} = 228 η_{100} = 270	η_{40} = 368 η_{100} = 418	132	115	This work
β-$Ni(OH)_2$/NF	1.0 M KOH	Facile hydrothermal etching method	η_{50} = 329	η_{50} = 170	40	51	[53]
Ni/NiO@rGO	0.5 M H_2SO_4	Chemical method	η_{10} = 480	η_{10} = 582	41	63	[54]
$Ni(OH)_2/NiCo_2O_4$	1 M KOH	One-step hydrothermal	η_{10} = 224	η_{10} = 189	43	41	[55]
S–Ni(Fe)OOH	1 M KOH	Chemical method	198	22	17.50	93.21	[56]
Ni–$Ni(OH)_2$	1.0 M KOH	Electrodeposition approach	– –	η_{10} = 73 η_{100} = 336	–	33	[57]
NF–$Ni(OH)_2$-Ni^{vac}Fe-LDHs	1 M KOH	Two-step hydrothermal method	η_{200} = 376	η_{200} = 247	121.37	95.87	[58]
$Ni_3S_2/Ni(OH)_2$	1 M KOH	Electrodeposition	η_{20} = 249	η_{10} = 66	61	59	[59]
Mo–$Ni(OH)_2/Fe_xNi_y(OH)_{3x+2y}$	1 M KOH	Hydrothermal method	η_{10} = 229	η_{10} = 57	33.53	75.31	[60]
NiO nanosheets	1 M KOH	Hydrothermal method	380	83	299	209	[61]

using the electrochemical workstation. Electrocatalytic materials synthesized via the ultrasonication excitation pathway are exceptional for use in the process of water splitting (OER/HER) due to their high electrochemically active surface area of 4.1 cm^2 for $Ni_2O_2(OH)$ and 6 cm^2 for $Ni_2O_2(OH)$/CNTs. When CNTs were introduced into the as-prepared $Ni_2O_2(OH)$, the water-splitting ability of the resulting $Ni_2O_2(OH)$/CNTs nanocomposite was effectively enhanced as they affected the electronic properties of the catalyst. The lowest overpotential (228 mV; 270 mV and 368 mV; 418 mV for OER and HER, respectively, at current density 40 and 100 $mAcm^{-2}$), minimum tafel slope, reduced charge transfer resistance value (2.9 Ω), lesser flat band potential (0.55 V), excellent exchange current density (2.2 $mAcm^{-2}$), and higher carrier concentration (14.7×10^{22} cm^{-3}) reveal the superior bifunctional water splitting performance of $Ni_2O_2(OH)$/CNTs material as compared to $Ni_2O_2(OH)$. Its excellent performance can be attributed to an exceptionally conductive substrate network provided by carbon-based materials (CNTs), which are effective for introducing more active sites, excellent electron mobility, and a greater exposed surface area.

Declaration of Competing interest

No conflict of interest

Acknowledgements

The authors acknowledge the financial support from Princess Nourah bint Abdulrahman University Researchers Supporting Project number (PNURSP2024R230), Princess Nourah bint Abdulrahman University, Riyadh, Saudi Arabia. Prof. Dr. Sonia Zulfiqar is highly thankful for the support provided by the Statutory City of Ostrava, Czechia through Research Grant “Global Experts”. Profs. Cochran and Zulfiqar are grateful for XPS measurements provided by Dr. Dapeng Jing of the Materials Analysis and Research Laboratory of the Iowa State University Office of Biotechnology and also to the National Science Foundation for financial support through research grant NSF-2113695.

References

[1] Strielkowski W, Civín L, Tarkhanova E, Tvaronavičienė M, Petrenko Y. Renewable energy in the Sustainable Development of electrical power sector: a review. Energies 2021;14:8240.
[2] Afaq M, Shahid M, Ahmad I, Yousaf S, Alazmi A, Mahmoud MHH, et al. Large-scale sonochemical fabrication of a Co_3O_4–$CoFe_2O_4$@MWCNT bifunctional electrocatalyst for enhanced OER/HER performances. RSC Adv 2023;13:19046–57.
[3] Chaudhary K, Basha B, Zulfiqar S, Yousaf S, Cochran EW, Al-Buriahi MS, et al. 3D cellular lattice like-Ti_3C_2 MXene based aerogels embedded with metal selenides particles for energy storage and water splitting applications. Fuel 2023;351:128856.
[4] Perera F. Pollution from fossil-fuel combustion is the leading environmental threat to global pediatric health and equity: solutions exist. Int J Environ Res Publ Health 2018;15:16.
[5] Farooq A, Khalil S, Basha B, Habib A, Al-Buriahi MS, Warsi MF, et al. Electrochemical investigation of C-doped $CoFe_2O_4$/Fe_2O_3 nanostructures for efficient electrochemical water splitting. Int J Hydrogen Energy 2024;51:1318–32.
[6] Gielen D, Boshell F, Saygin D, Bazilian MD, Wagner N, Gorini R. The role of renewable energy in the global energy transformation. Energy Strategy Rev 2019;24:38–50.
[7] Katubi KM, Warsi A-Z, Aziz F, Khattak ZAK, Warsi MF, Al-Buriahi MS, et al. Tungsten oxide-copper oxide supported on reduced graphene oxide as a proficient electrocatalyst with enhanced hydrogen evolution efficiency in an alkaline media. Curr Appl Phys 2023;51:80–90.
[8] Yue M, Lambert H, Pahon E, Roche R, Jemei S, Hissel D. Hydrogen energy systems: a critical review of technologies, applications, trends and challenges. Renew Sustain Energy Rev 2021;146:111180.
[9] Rosen MA, Koohi-Fayegh S. The prospects for hydrogen as an energy carrier: an overview of hydrogen energy and hydrogen energy systems. Energy, Ecology and Environment 2016;1:10–29.
[10] Qin H, Ye Z, Wei X, Liu X, Liu X, Fan J, et al. Bifunctional electrolyzation for simultaneous organic pollutant degradation and hydrogen generation. ACS ES&T Engineering 2021;1:1360–8.
[11] Youssef N, Amal A. Hydrogen generation by water electrolysis. In: Murat E, editor. Advances in hydrogen generation technologies. Rijeka: IntechOpen; 2018. Ch. 1.
[12] Wang S, Lu A, Zhong C-J. Hydrogen production from water electrolysis: role of catalysts. Nano Convergence 2021;8:4.
[13] Sabir AS, Pervaiz E, Khosa R, Sohail U. An inclusive review and perspective on Cu-based materials for electrochemical water splitting. RSC Adv 2023;13:4963–93.
[14] Sheng M, Yang Y, Bin X, Que W. One-Step electrochemical synthesis and surface reconstruction of NiCoP as an electrocatalyst for bifunctional water splitting. Materials 2023;16:1529.
[15] Tahir T, Chaudhary K, Warsi MF, Saif MS, Alsafari IA, Shakir I, et al. Synthesis of sponge like Gd^{3+} doped vanadium oxide/2D MXene composites for improved degradation of industrial effluents and pathogens. Ceram Int 2022;48:1969–80.
[16] Li C, Baek J-B. Recent advances in noble metal (Pt, Ru, and Ir)-Based electrocatalysts for efficient hydrogen evolution reaction. ACS Omega 2020;5:31–40.
[17] Yousaf S, Zulfiqar S, Somaily HH, Warsi MF, Rasheed A, Shahid M, et al. An efficient and stable iodine-doped nickel hydroxide electrocatalyst for water oxidation: synthesis, electrochemical performance, and stability. RSC Adv 2022;12:23454–65.
[18] Niu H, Wang Q, Huang C, Zhang M, Yan Y, Liu T, et al. Noble metal-based heterogeneous catalysts for electrochemical hydrogen evolution reaction. Appl Sci 2023;13:2177.
[19] Banoth P, Kandula C, Kollu P. Introduction to electrocatalysts. Noble metal-free electrocatalysts: new trends in electrocatalysts for energy applications, vol. 2. American Chemical Society; 2022. p. 1–37.
[20] Lee G, Jun SE, Kim Y, Park I-H, Jang HW, Park SH, et al. Multicomponent metal oxide- and metal hydroxide-based electrocatalysts for alkaline water splitting. Materials 2023;16:3280.
[21] Cai Q, Hong W, Jian C, He X, Liu W. Recent development of self-supported alkaline hydrogen evolution reaction electrocatalysts for industrial electrolyzer. Advanced energy and sustainability Research.n/a:2200178.
[22] Wang Y, Zhang Z, Mao Y, Wang X. Two-dimensional nonlayered materials for electrocatalysis. Energy Environ Sci 2020;13:3993–4016.
[23] Yousaf S, Katubi KM, Zulfiqar S, Warsi MF, Alrowaili ZA, Al-Buriahi MS, et al. Modulating electronic and structural properties of NiCo- layered double hydroxide with iodine: as an efficient electro-catalyst for the oxygen evolution reaction. Int J Hydrogen Energy 2023;48:27201–14.
[24] Zang Y, Lu DQ, Wang K, Li B, Peng P, Lan YQ, et al. A pyrolysis-free Ni/Fe bimetallic electrocatalyst for overall water splitting. Nat Commun 2023;14:1792.
[25] Zhao D, Dai M, Zhao Y, Liu H, Liu Y, Wu X. Improving electrocatalytic activities of $FeCo_2O_4$@$FeCo_2S_4$@PPy electrodes by surface/interface regulation. Nano Energy 2020;72:104715.
[26] Hassan M, Baig MM, Yousaf S, Faheem M, Hussain A, Niaz B, et al. Efficient water splitting catalyst: low-temperature selenization of Co and Ni hydroxide nanosheets on carbon cloth for enhanced electro-catalytic activity. Diam Relat Mater 2023;139:110298.
[27] Osgood H, Devaguptapu SV, Xu H, Cho J, Wu G. Transition metal (Fe, Co, Ni, and Mn) oxides for oxygen reduction and evolution bifunctional catalysts in alkaline media. Nano Today 2016;11:601–25.
[28] Qiu H-J, Fang G, Gao J, Wen Y, Lv J, Li H, et al. Noble metal-free nanoporous high-entropy alloys as highly efficient electrocatalysts for oxygen evolution reaction. ACS Mater Lett 2019;1:526–33.
[29] Cao Y. Roadmap and direction toward high-performance MoS_2 hydrogen evolution catalysts. ACS Nano 2021;15:11014–39.
[30] Angeles-Olvera Z, Crespo-Yapur A, Rodríguez O, Cholula-Díaz JL, Martínez LM, Videa M. Nickel-based electrocatalysts for water electrolysis. Energies 2022;15:1609.
[31] Niyitanga T, Evans PE, Ekanayake T, Dowben PA, Jeong HK. Carbon nanotubes-molybdenum disulfide composite for enhanced hydrogen evolution reaction. J Electroanal Chem 2019;845:39–47.
[32] Kumar A, Yasin G, Vashistha VK, Das DK, Rehman MU, Iqbal R, et al. Enhancing oxygen reduction reaction performance via CNTs/graphene supported iron protoporphyrin IX: a hybrid nanoarchitecture electrocatalyst. Diam Relat Mater 2021;113:108272.
[33] Xue H, Yang T, Zhang Z, Zhang Y, Geng Z, He Y. Stimulate the hidden catalysis potential and exposure of nickel site in NiSe@CNTs result in ultra-high HER/OER activity and stability. Appl Catal B Environ 2023;330:122641.
[34] Altay R, Sadaghiani AK, Sevgen MI, Şişman A, Koşar A. Numerical and experimental studies on the effect of surface roughness and ultrasonic frequency on bubble dynamics in acoustic cavitation. Energies 2020;13:1126.
[35] Pokhrel N, Vabbina PK, Pala N. Sonochemistry: science and engineering. Ultrason Sonochem 2016;29:104–28.
[36] Rehman S, Almessiere MA, Al-Suhaimi E A, Hussain M, Yousuf Bari M, Mehmood Ali S, et al. Ultrasonic synthesis and biomedical application of $Mn_{0.5}Zn_{0.5}Er_xY_xFe_{2-2x}O_4$ nanoparticles. Biomolecules 2021;11:703.
[37] Kite SV, Kadam AN, Sathe DJ, Patil S, Mali SS, Hong CK, et al. Nanostructured TiO_2 sensitized with MoS_2 nanoflowers for enhanced photodegradation efficiency toward methyl orange. ACS Omega 2021;6:17071–85.
[38] Wu J, Lee G. Sonochemical synthesis of zinc sulfide photocatalysts and their environmental applications. Handbook of ultrasonics and sonochemistry. Singapore: Springer; 2016. p. 867–99.
[39] Zhang R, Li Y, Zhou X, Yu A, Huang Q, Xu T, et al. Single-atomic platinum on fullerene C60 surfaces for accelerated alkaline hydrogen evolution. Nat Commun 2023;14:2460.
[40] Ye C, Wang M-Q, Bao S-J, Ye C. Micropore-boosted layered double hydroxide catalysts: EIS analysis in structure and activity for effective oxygen evolution reactions. ACS Appl Mater Interfaces 2019;11:30887–93.
[41] Khdary NH, El Enany G, Almalki AS, Alhassan AM, Altamimi A, Alshihri S. Preparation of Cu/Sn-organic nano-composite catalysts for potential use in

hydrogen evolution reaction and electrochemical characterization. Nanomaterials 2023;13:911.
[42] Wang Z, Zhao P, Li P, Li S, Liao L, Luo Y, et al. Hierarchical cerium oxide anchored multi-walled carbon nanotube hybrid with synergistic effect for microwave attenuation. Compos B Eng 2019;167:477–86.
[43] Shahid MY, Asghar M, Arbi HM, Zafar M, Ilyas SZ. Role of magnesium in ZnS structure: Experimental and theoretical investigation. AIP Adv 2016;6.
[44] Roy S, Das TK. Protein capped silver nanoparticles from fungus: X-ray Diffraction Studies with Antimicrobial properties against bacteria. Int J ChemTech Res 2015;7:1452–9.
[45] Bindu P, Thomas S. Estimation of lattice strain in ZnO nanoparticles: X-ray peak profile analysis. Journal of Theoretical and Applied Physics 2014;8:123–34.
[46] Mao Y, Zhou B, Peng S. Simple deposition of mixed α, β-nickel hydroxide thin film onto nickel foam as high-performance supercapacitor electrode material. J Mater Sci Mater Electron 2020;31:9457–67.
[47] Shruthi B, Madhu B, Raju VB, Vynatheya S, Devi BV, Jayashree G, et al. Synthesis, spectroscopic analysis and electrochemical performance of modified β-nickel hydroxide electrode with CuO. J Sci: Advanced Materials and Devices 2017;2:93–8.
[48] Budipramana Y, Ersam T, Kurniawan F. Synthesis nickel hydroxide by electrolysis at high voltage. ARPN J Eng Appl Sci 2014;9:2074–7.
[49] Tang Q, Li B, Ma W, Gao H, Zhou H, Yang C, et al. Fabrication of a double-layer membrane cathode based on modified carbon nanotubes for the sequential electro-Fenton oxidation of p-nitrophenol. Environ Sci Pollut Control Ser 2020;27:18773–83.
[50] Xiao Z, Huang YC, Dong CL, Xie C, Liu Z, Du S, et al. Operando identification of the dynamic behavior of oxygen vacancy-rich $Co_{(3)}O_{(4)}$ for oxygen evolution reaction. J Am Chem Soc 2020;142:12087–95.
[51] Liu S, Kang L, Hu J, Jung E, Zhang J, Jun SC, et al. Unlocking the potential of oxygen-deficient copper-doped Co_3O4 nanocrystals confined in carbon as an advanced electrode for flexible solid-state supercapacitors. ACS Energy Lett 2021;6:3011–9.
[52] Xiong D, Li W, Liu L. Vertically aligned porous nickel(II) hydroxide nanosheets supported on carbon paper with long-term oxygen evolution performance. Chem Asian J 2017;12:543–51.
[53] Yang J-H, Xu X, Chen M, Yang D, Lu H, Sun Y, et al. Morphology-controllable nanocrystal β-$Ni(OH)_2$/NF designed by hydrothermal etching method as high-efficiency electrocatalyst for overall water splitting. J Electroanal Chem 2021;882:115035.
[54] Narwade SS, Mali SM, Digraskar RV, Sapner VS, Sathe BR. Ni/NiO@ rGO as an efficient bifunctional electrocatalyst for enhanced overall water splitting reactions. Int J Hydrogen Energy 2019;44:27001–9.
[55] Sang Y, Cao X, Wang L, Ding G, Wang Y, Yu D, et al. Facile synthesis of three-dimensional spherical $Ni(OH)_2/NiCo_2O_4$ heterojunctions as efficient bifunctional electrocatalysts for water splitting. Int J Hydrogen Energy 2020;45:30601–10.
[56] Li Q, Chen B, Huang L, Zhu S, Qian Y, Wu D, et al. S-doped Ni (Fe) OOH bifunctional electrocatalysts for overall water splitting. Int J Hydrogen Energy 2024;51:1392–406.
[57] Zhang W, Yin Q, Zhang Y, Peng S, Li Y. Electrodeposited crystalline-amorphous Ni-Ni $(OH)_2$ electrocatalysts for efficient hydrogen evolution via alkaline water splitting. J Alloys Compd 2023;948:169727.
[58] Mu W, Bao D, Chang C. Growth of nickel vacancy NiFe-LDHs on Ni $(OH)_2$ nanosheets as highly efficient bifunctional electrocatalyst for overall water splitting. Int J Hydrogen Energy 2022;47:15603–11.
[59] Wang H, Wang C, Zhang W, Yao S. A nano-spherical structure Ni_3S_2/Ni $(OH)_2$ electrocatalyst prepared by one-step fast electrodeposition for efficient and durable water splitting. Int J Hydrogen Energy 2022;47:14916–29.
[60] Liu Y, Ding M, Qin Y, Zhang B, Zhang Y, Huang J. Crystalline/Amorphous Mo-Ni $(OH)_2/Fe_xNi_y$ $(OH)_{3x+2y}$ hierarchical nanotubes as efficient electrocatalyst for overall water splitting. J Colloid Interface Sci 2024;657:219–28.
[61] Mishra RK, Kumar V, Choi GJ, Ryu JW, Mane SM, Shin JC, et al. Hexagonal NiO nanosheets on Ni-foam as an electrocatalyst for high-performance water splitting application. Mater Lett 2022;324:132740.